13th ANKARA INTERNATIONAL AEROSPACE CONFERENCE **AIAC-2025-117**
17-19 September 2025 - METU, Ankara, TURKIYE

INVESTIGATION OF SECONDARY FLOW LOSSES IN LOW PRESSURE TURBINES WITH A NOVEL ENDWALL FEATURE

Emrullah YILMAZ*
Navist Engineering
Ankara Yildirim Beyazit University
Ankara, Türkiye

Oguzhan MURAT†
Ankara Yildirim Beyazit University
Ankara, Türkiye

ABSTRACT

The phenomenon of secondary flows has been a significant subject of study in turbomachinery for decades. Scientists and engineers have conducted numerous experimental and numerical investigations to understand and optimize the losses caused by secondary flows. Most frequently studied methods include endwall contouring. However, with the recent advances in manufacturing techniques, a wider range of options is now available.

In this study, three different endwall features are studied using 3D steady-state RANS simulations to examine their influence on secondary flow losses. The first two are conventional techniques, namely riblets and fillets placed on the hub. The third one explores a novel idea that incorporates a channel embedded inside the hub. This channel opening starts at the passage inlet and merges back with the passage at the exit. It is observed in the kinetic energy loss coefficient that the novel channel method outperforms the conventional endwall contouring methods, reducing the magnitude of the core secondary flow by about 32% compared to the baseline (smooth) case.

INTRODUCTION

Secondary flows in turbomachinery is a complex phenomenon, caused by the interaction between the endwall and the blade geometry. In turbomachinery applications, the growing boundary layer of the endwall clashing with the turbine/compressor blades creates a vortex starting from the root of the blades leading edge. This vortex grows in size as it passes the blade passage and detaches from the endwall, causing aerodynamic losses by reducing the lift of the turbine blades. In a review paper by Langston [Langston, 2001], details about the studies made in secondary flow losses from 1985 to the start of 2000's are provided. This paper also dwells on the reduction techniques of secondary flow losses. Some of these techniques are the use of fences and grooves in the endwall and suction side surface of the blade, endwall contouring with non-planar profiles and leading edge junction modifications. These modifications aim to reduce the loss generated by the passage vortex, by means of manipulating the boundary layer in the endwall and exploiting the interaction between passage vortex and the smaller vortices.

In a study by Sauer et al. [Sauer, Müller and Vogeler, 2000] the effect of leading edge bulbs was

*Graduate Student & CFD Project Engineer, Email: emrullah.yilmaz@navist.com.tr
†Assistant Professor of Aerospace Engineering, Email: oguzhan.murat@aybu.edu.tr

Table 1: Geometry of SPLEEN C1 Cascade From Ref.[Lopes and Filipe, 2024]

True Chord (C)	52.28	[mm]
Axial Chord (C_{ax})	47.614	[mm]
Span (H)	165	[mm]
Pitch (g)	32.95	[mm]
Inlet Metal Angle ($\alpha_{met,in}$)	37.3	[°]
Outlet Metal Angle ($\alpha_{met,out}$)	53.8	[°]

examined both experimentally and numerically on the established test case of T106. In this study, a variety of bulb sizes were studied and a significant reduction in the secondary flow losses were achieved thanks to the weakening of the passage vortex. In a similar work by Saha et al. [Saha, Mahmood and Acharya, 2006] the effect of adding a fillet to the leading edge of the blades junction was examined. This study showed the effect of linear and circular fillet profiles and compared these results with the baseline endwall. The study reported a reduction in vorticity of the passage vortex and suction side leg vortex. In a study by Zhang et al. [Zhang, Miao, Jiang and Qi, 2014], the addition of riblets on the endwall was studied using experimental and numerical techniques. With the presented CFD studies, it was reported that the addition of riblets decreases the lift off distance of the passage vortex. Presented experimental results also support this conclusion. In a different study by Dickel et al. [Dickel, Marks, Christopher, Sondergaard and Wolff, 2018] the effect of non-planar endwall contouring was examined using RANS simulations and experimental measurements. In this study, a decrease in the size and strength of the passage vortex was reported by containing the said vortex in a valley shaped endwall.

In this study, three different endwall features inspired by the studies presented in [Zhang, Miao, Jiang and Qi, 2014], [Saha, Mahmood and Acharya, 2006] and a novel feature will be examined by using 3D RANS simulations, and their influence on the secondary flow losses will be compared using the newly established SPLEEN C1 Test Case provided by [Lavagnoli, Lopes, Simonassi and Torre, 2024] and the corresponding CFD simulations.

SPLEEN C1 TEST CASE

Secondary and Leakage Flow Effects in High-Speed Low-Pressure Turbines (SPLEEN) project is a relatively new high speed low pressure turbine cascade test case, designed by von Karman institute in collaboration with Safran Aeroengines. Test case flow conditions range from 0.7-0.95 Mach (M) and 65k-120k Reynolds Number (Re) which represents a wide range of flow conditions. Data from the test case is openly available in [Lavagnoli, Lopes, Simonassi and Torre, 2024] which also houses the comprehensive report of the test case by [Lopes and Filipe, 2024]. Schematics of the SPLEEN blade can be found in Fig.1. The corresponding geometric details of the blade can be found in Table 1. Axial Chord (C_{ax}), Span (H) and Pitch (g) values are used in the non-dimensionalization of the test results.

Pressure readings 0.5C_{ax} downstream of the blade trailing edge (Plane 6) are processed further to investigate the characteristics of secondary flows using the kinetic energy loss equation given in Eq.1 taken from [Lopes and Filipe, 2024], where, P_6, P_{06}, P_{01}, γ are downstream static pressure, downstream total pressure, inlet total pressure and heat capacity ratio respectively. Using the Eq.1 allows us to identify the kinetic energy loss generation caused by secondary flows.

$$\xi = 1 - \frac{1 - (\frac{P_6}{P_{06}})^{\frac{\gamma-1}{\gamma}}}{1 - (\frac{P_6}{P_{01}})^{\frac{\gamma-1}{\gamma}}} \tag{1}$$

Readings from pressure taps on the blade is used to calculate the isentropic mach number M_{isen}, given in Eq.2. P_{tot} value for the calculation of M_{isen} is taken as the inlet total pressure P_{01}. Static pressure values are taken as the static pressure at the surface of the blade.

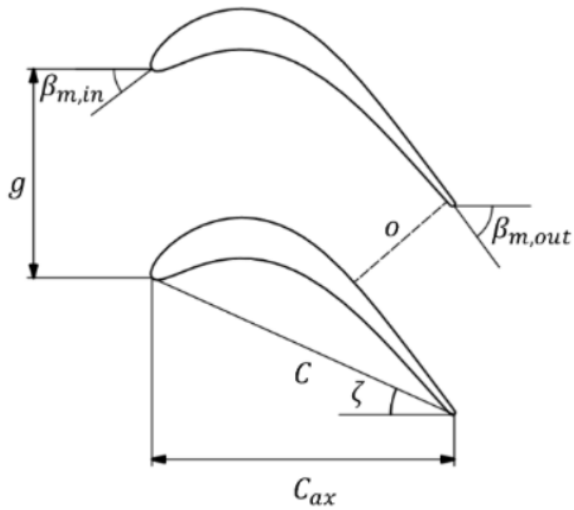

Figure 1: Schematic View of SPLEEN C1 Cascade [Lopes and Filipe, 2024]

$$M(P_{tot}, P_{stat}) = \sqrt{\frac{2}{\gamma - 1}\left[\left(\frac{P_{stat}}{P_{tot}}\right)^{-\frac{\gamma-1}{\gamma}} - 1\right]} \tag{2}$$

Examining the test results provided in Ref.[Lavagnoli, Lopes, Simonassi and Torre, 2024], the effect of secondary flow losses can be examined. Secondary flows cause a reduction in the lift generated by the turbine blades. This effect can be seen with the M_{isen} value on the wing surface. Graphs of M_{isen} with respect to the axial location (x/C_{ax}) for different spanwise locations z/H, is given in Fig.2. As can be seen in the graph, the area between the graphs gets smaller in proximity of the endwall, which shows a drop in lift due to the effect of secondary flows.

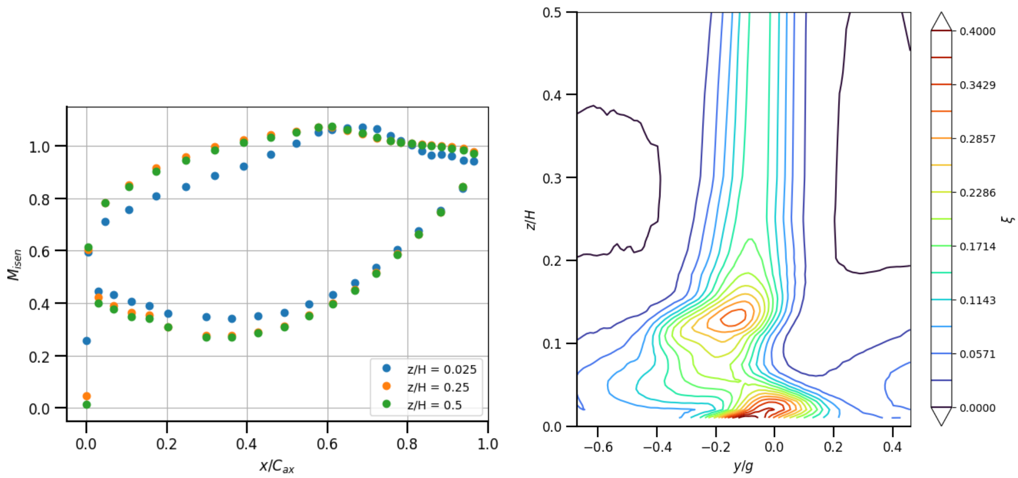

Figure 2: Isentropic Mach Number Distribution on the Surface of the Blade (Left) Kinetic Energy Loss Coefficient (ξ) Contour at P_6 (Right) [Lavagnoli, Lopes, Simonassi and Torre, 2024]

With the static and total pressure measurements 0.5C_{ax} downstream of the blade trailing edge (Plane 6), a contour plot for the kinetic energy loss ξ can be constructed, described by Denton[Denton, 1993], for the measured data in Ref.[Lavagnoli, Lopes, Simonassi and Torre, 2024], using the Eq.1. Examining the contour in Fig.2, we can see the passage vortex as the big region of energy loss formed at about $z/H = 0.13$. There is also a higher loss region which signifies the existence of a smaller vortical structure close to the endwall.

Table 2: Boundary Conditions

Inlet Boundary Conditions		
Total Pressure (P_{01})	16285	[Pa]
Total Temperature (T_{01})	300	[K]
Turbulent Intensity	0.026	
Turbulent Length Scale	0.93	[mm]
Outlet Boundary Conditions		
Static Pressure (P_6)	9629	[Pa]
Static Temperature (T_6)	258.18	[K]
Turbulent Intensity	0.026	
Turbulent Length Scale	0.93	[mm]

METHODOLOGY

In this section, the methodology of study will be detailed with the mesh independence study and validation of the CFD model. Reynolds-averaged Navier-Stokes (RANS) simulations of the SPLEEN C1 LPT Linear Cascade have been performed with the CFD software Star-CCM+, a commercial Finite Volume CFD software. RANS equations are solved using the Implicit Coupled solver of Star-CCM+ for pressure-velocity coupling. Ideal Gas model with Sutherland's Law for viscosity is used to model the air. $k-\omega$ SST model with γ-Re_θ transition model developed by [Langtry and Menter, 2009] is used for the turbulence closure. This decision was made in light of the study of [Rosafio, Lopes, Salvadori, Lavagnoli, Misul, 2012], where they studied the separation prediction performance of different transition models on the SPLEEN C1 cascade. It is observed by Rosafio et.al.[Rosafio, Lopes, Salvadori, Lavagnoli, Misul, 2012] that using the γ-Re_θ provides better accuracy in resolving the flow separation that occurs on the turbine blades with respect to the other RANS models.

CFD Studies of the Test Case

Experimental data provided by Lopes[Lopes and Filipe, 2024] is used for the validation of the test case CFD studies. The boundary conditions for total pressure at inlet, static pressure at outlet and turbulence properties are also taken from [Lopes and Filipe, 2024] for test case with $M_{out,is} = 0.9Ma$ and $Re_{out} = 120k$. Numerical values of the boundary conditions can be found in Table 2, static temperature at the outlet is calculated using the isentropic relation as given in Eq.3.

$$\frac{T_6}{T_{01}} = (1 + \frac{\gamma - 1}{2} M^2)^{-1} \tag{3}$$

Only one passage of the turbine cascade is modeled as the geometry of the cascade is periodic. A wireframe of the CFD domain can be seen in Fig.3

All of the boundaries and the size of the domain can be seen in Fig.3. The 3D domain is created to cover the half span of $z/H = 0.5$ and the boundary condition at $z/H = 0.5$ is given as symmetry.

Mesh Independency Study:

Meshes used in the study are created using the inbuilt automated meshing tool in Star-CCM+. This tool is able to create polyhedral cells with prism layers (boundary layer mesh) in a given domain and is able to create fully conformal surface meshes for periodic boundaries which is important for eliminating interpolation errors that can cause inaccuracies while obtaining a CFD solution. For this study *polyhedral mesher* and *advancing layer mesher* of Star-CCM+ is used to create the 3D polyhedral cells and the prism (boundary) layers respectively. A mesh independence study is conducted to find the mesh sizes that accurately model the problem. Four different meshes are created for this study ranging from a coarse mesh with 2.3 million cells and a very fine mesh with 10.4 million cells. These meshes are obtained by varying the base size of the meshes while keeping the boundary layer total thickness and number of prism layers identical. This was done to keep the

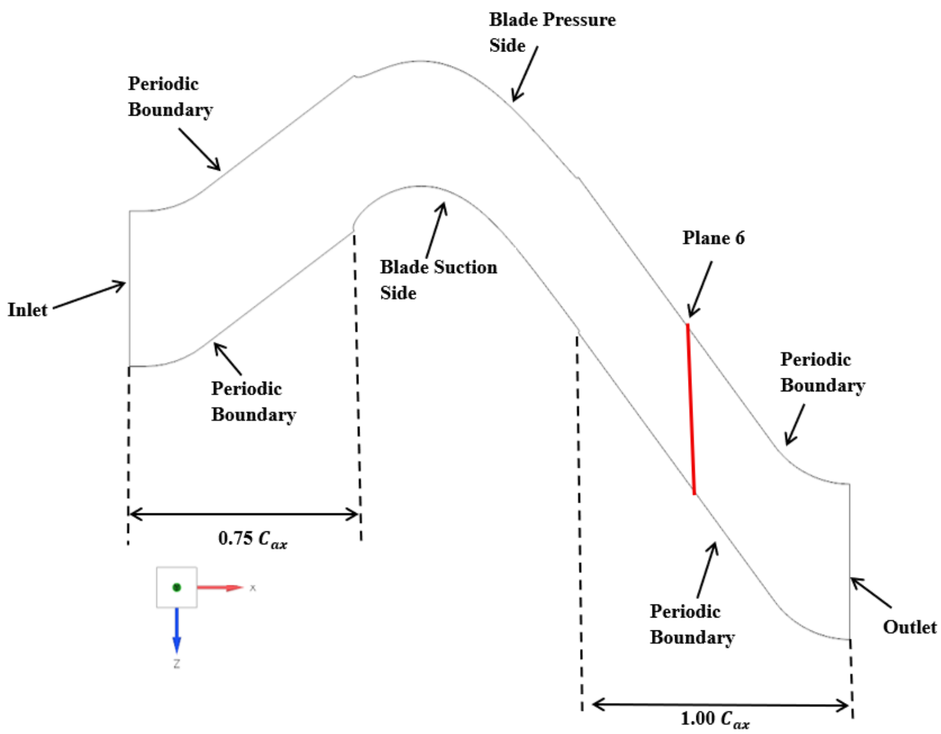

Figure 3: Wireframe of the Created CFD Domain

Table 3: Mesh Independency Results

Kinetic Energy Loss (ξ)		
Mesh Size	**max ξ**	**Distance to End-Wall**
Coarse (2.3M)	0.375	14.62 mm
Medium (3.9M)	0.413	15.13 mm
Fine (5M)	0.441	14.63 mm
Very Fine (10.4M)	0.432	13.35 mm
Experiment	0.330	21.15 mm

y+ value constant throughout all of the meshes. Using 3 mm boundary layer total thickness and 17 prism layers with a layer growth rate of 1.2 yielded a mesh with a $y+ \approx 1.7$. After simulations achieved convergence, isentropic mach number (M_{isen}) on the blade surfaces at different spanwise locations are calculated using the isentropic relation given in Eq.2. Kinetic Energy Loss coefficient (ξ) is calculated using Eq.1 from a plane $0.5C_{ax}$ downstream of the blade trailing edge (Plane 6). Evaluations of the maximum Kinetic Energy Loss (ξ) in the vortex core can be found in Table 3.

From Table 3, it can be seen that the fine and very fine meshes provide similar results with respect to the maximum ξ value, but compared to the experimental results, they overestimate the loss coefficient at the core of the passage vortex, and underestimate the distance of the vortex core from the endwall. This behaviour of RANS based turbulence closure models is well documented in the work of [Pichler, Zhao, Sandberg, Michelassi, Pacciani, Marconcini and Arnone, 2019] and [Marconcini, Pacciani, Arnone, Michelassi, Pichler, Zhao and Sandberg, 2019]. In both studies it can be seen that the RANS closure models overpredict the magnitude of loss compared to the LES studies. In his thesis [Lopes and Filipe, 2024], it is stated that the reason for this over-prediction is the Boussinesq approximation that is at the heart of the RANS turbulence models. Therefore, while the κ-ω SST with γ-Re_θ transition model represents a reasonable compromise between computational cost and accuracy, its predictions in secondary flow zones should be interpreted with caution.

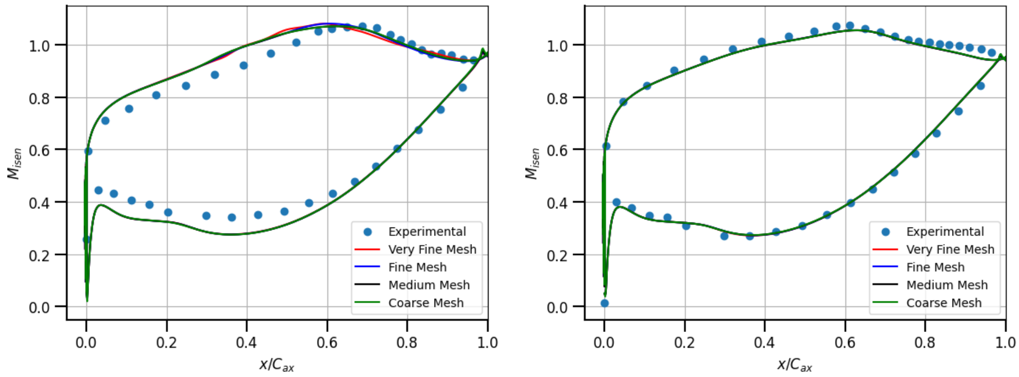

Figure 4: Isentropic Mach Number on the Blade Surfaces at $z/H = 0.025$ (Left) and $z/H = 0.5$ (Right)

Results of the comparison of M_{isen} on blade surfaces in Fig.4, show that the presented CFD model is able to accurately model the flow outside the effects of the endwall, but the model shows discrepancies close to the wall. This could be due to the earlier mentioned limitation of the RANS turbulence closure and requires further investigation. From the graph on the left in Fig4, it can be concluded that refining the mesh does not meaningfully affect the pressure distribution on the blade surfaces closer to the endwall.

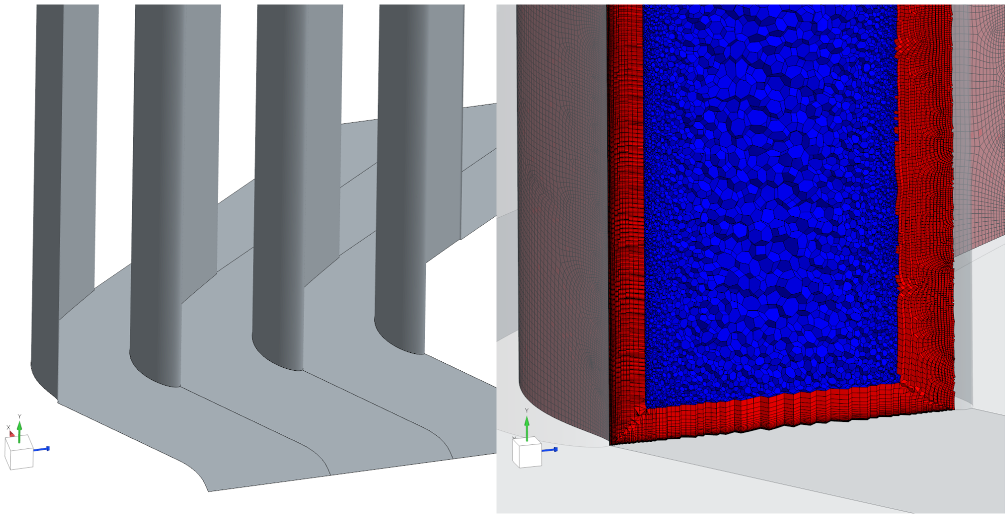

Figure 5: Test Case Geometry (Left) Generated Mesh for a Passage (Right)

Upon these examinations the fine mesh is chosen for the rest of the study because coarse and medium mesh sizes failed to capture some the geometric details of the endwall features presented in the coming sections. This mesh also provides grid independence as the numerical results of maximum ξ values are about 2% of each other for fine and very fine meshes. This mesh can be seen in Fig.5. Boundary layers created by the software are highlighted in red while the core mesh of the domain volume is highlighted in blue.

Cell quality metrics of this mesh is judged using the guidelines provided by STAR-CCM+. The judged metrics are skewness angle, cell quality and volume change ratio. The skewness angle is the angle between the face area vector(face normal) and the vector connecting the two cell centroids. An angle of zero indicates a perfectly orthogonal mesh. Skewness angles higher than 90° results in convergence issues due to diffusion terms in the calculations. In our case the maximum skewness angle present in the mesh is 70°, which is adequate and did not cause any convergence problems in the solution.

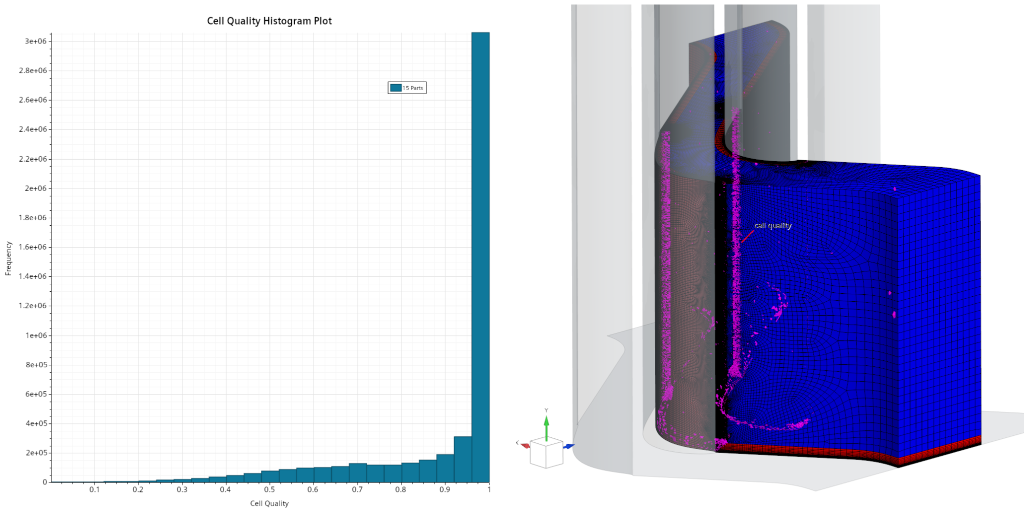

Figure 6: Cell Quality Histogram Graph of the Fine Mesh

Cell quality is defined as a function not only of the relative geometric distribution of the cell centroids of the face neighbor cells, but also of the orientation of the cell faces. Generally, flat cells with highly non-orthogonal faces have a low cell quality. As seen in Fig.6, the fine mesh consists of mainly high quality cells. The mesh with quality smaller than 0.1 is highlighted in the mesh given in Fig.6. This shows that bad quality cells are mainly generated in clashing boundary layers of the blades and the endwall and between the transition of the boundary layer to the core mesh. But their numbers are quite small overall and unlikely to cause trouble.

Volume change in a mesh is defined as the volume ratio of a cell with respect to its neighbors. A value of 1.0 indicates that the cell has a volume equal to or higher than its neighbors. As the cell volume decreases relative to its neighbors (such as a sliver or flat cell), the volume change metrics decreases as well. A large jump in volume from one cell to another can cause potential inaccuracies and instability in the solvers. Cells with a volume change of 0.01 or lower are considered bad cells. As it stands there are no cells in the fine mesh with volume change value smaller than 0.01.

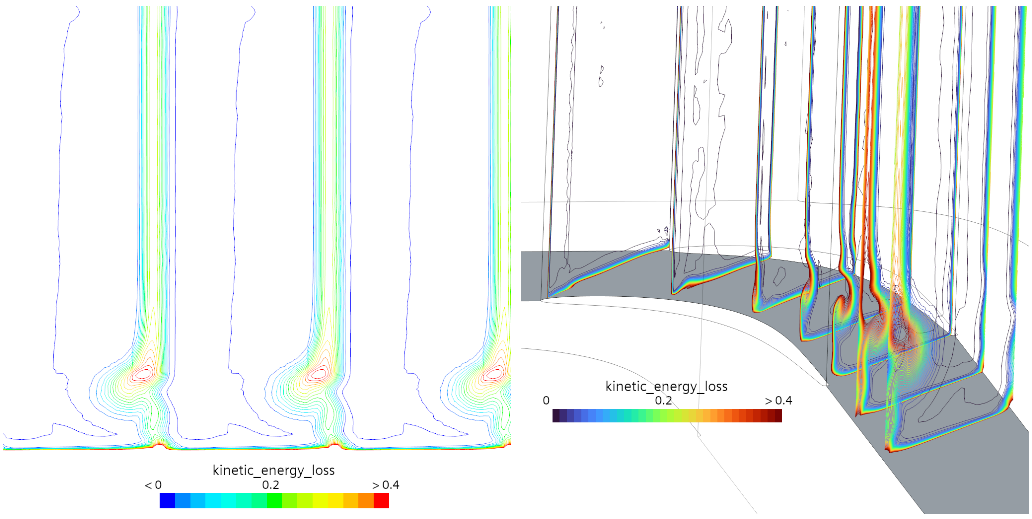

Figure 7: Kinetic Energy Loss Coefficient (ξ) Contour From Plane 6 (Left) Kinetic Energy Loss (ξ) Contours Along the Turbine Passage (Right)

For further investigation of the test case CFD, Fig.7 presents the contours of loss coefficient ξ. In the contour, it is easy to identify the big region of loss that is about 14 mm away from the endwall. This region can be identified as the passage vortex, which is the main contributor to the overall aerodynamic losses caused by secondary flows. To understand the phenomenon even further, ξ contours along the passage are also examined. This shows that the majortiy of the large vortex structures starts to form at about $0.3C_{ax}$ downstream of the leading edge, which corresponds to the axial location where the vortices emerging from the pressure side clashes with the suction side.

CFD RESULTS WITH DIFFERENT ENDWALL FEATURES

In this section, the CFD results obtained with the riblet, fillet and channel features will be presented and discussed. The same CFD model described in methodology section is used in the study of these features. Results from this test case CFD model will be compared with the results obtained in this section.

CFD Studies Of The Riblet Feature

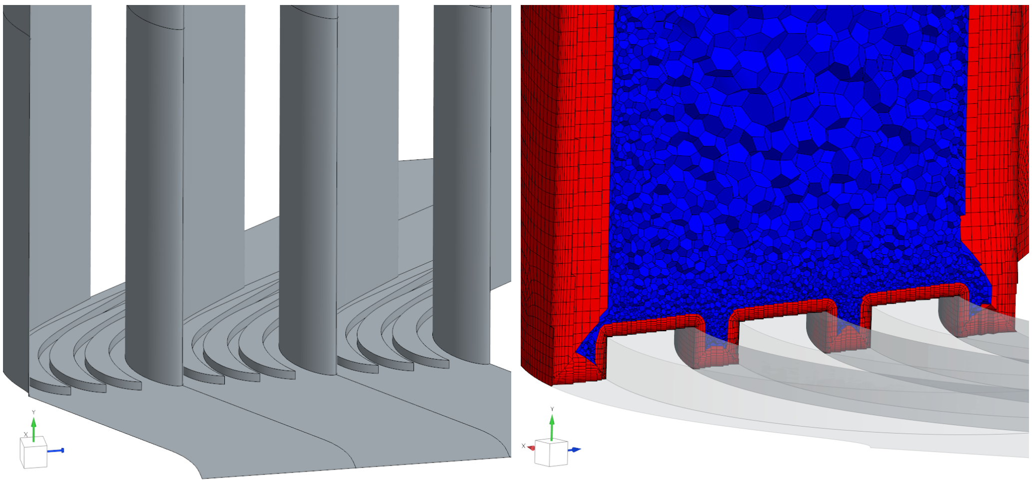

Figure 8: Riblet Feature (Left) Generated Mesh Around the Feature (Right)

As mentioned in the introduction, the riblet feature is inspired from the study of [Zhang, Miao, Jiang and Qi, 2014], where they implemented very small pyramid like details to their endwall to break the formation of the passage vortex. This feature was achieved using advanced manufacturing techniques. In our implementation of a similar feature, the blade section in the root is scaled and translated to the passage so it acts like a guide vane in the endwall. This feature and the generated finite volume mesh can be seen in more detail in Fig.8. Although it is not quite like the one presented in the work of [Zhang, Miao, Jiang and Qi, 2014], it still provides similar benefits seen in the reference work, mainly decreasing the lift off distance of the passage vortex from the endwall and decreasing the size and strength of the passage vortex. The CFD domain is created as before with the same meshing settings for the boundary layer, with only change being the reduced total thickness of the boundary layer in the riblet walls. This was done to reduce the collapsed boundary layer cells and improve mesh quality.

Kinetic energy loss contour obtained from the CFD studies of the riblet feature is given in Fig.9. With these geometric changes, it is observed that the passage vortex is significantly smaller and the lift off distance has dropped to 10.49mm with respect to the test case CFD study. Examining the Fig.9,it can be said that similar results seen in the work of [Zhang, Miao, Jiang and Qi, 2014] have been achieved in this study as well, including some smaller vortex structures forming due to the riblets. Upon examining the development of losses along the passage, given in Fig.9, it is seen that every rib creates its own vortical structures and all of these smaller vortices get mixed with passage vortex. However the existence of ribs in the way of the passage vortex, is still able to decrease the lift off distance and the size of the vortex.

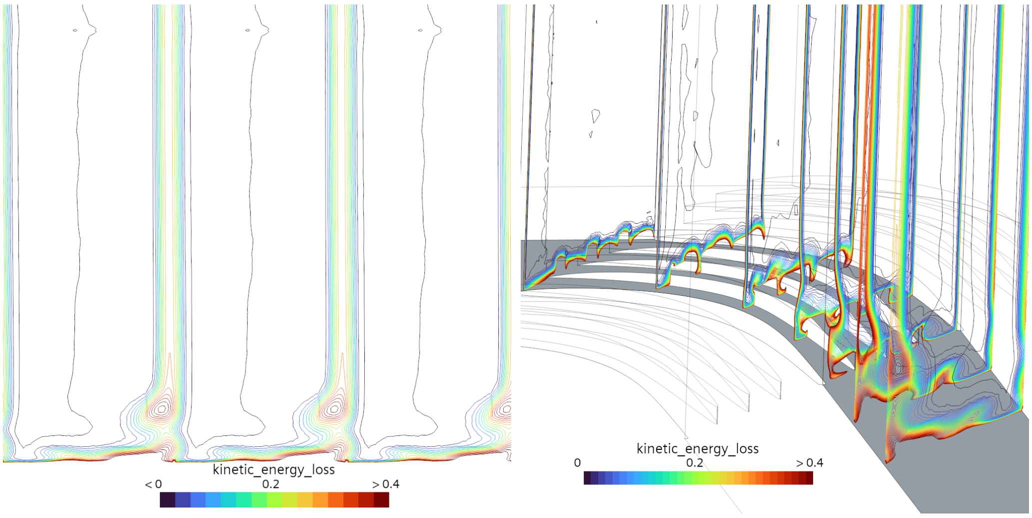

Figure 9: Kinetic Energy Loss Coefficient (ξ) Contour With the Riblet Feature (Left) Kinetic Energy Loss Coefficient (ξ) Contours Along the Passage (Right)

CFD Studies Of The Fillet Feature

As mentioned in the introduction, the fillet feature is inspired by the works of [Saha, Mahmood and Acharya, 2006] and [Sauer, Müller and Vogeler, 2000]. Both of these studies implemented a smooth feature on the leading edge of the turbine blades, to control the turn rate of the endwall boundary layer in the hopes of decreasing the strength of the passage vortex. Through their studies, they achieved significant improvements in reducing the strength of the passage vortex and a decrease in the passage vortex lift off distance.

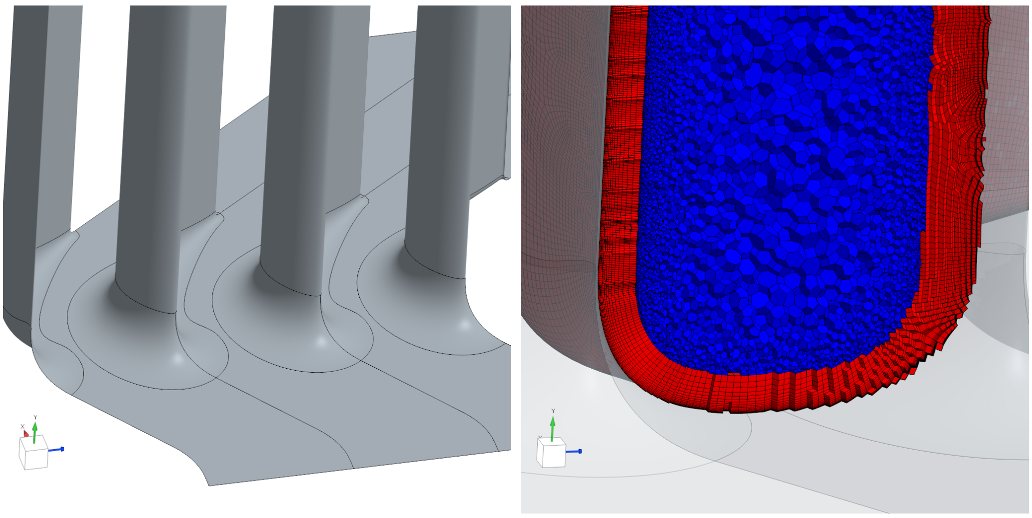

Figure 10: Fillet Feature (Left) Generated Mesh (Right)

From these inspirations, the geometry of this study is derived and can be seen in Fig.10. This feature created by filleting the root of the turbine blade with circular fillet varying along the axial chord C_{ax}. The fillet Starts with 12mm radius at the leading edge and goes down to 2mm at the trailing edge. This reduction in fillet radius happens linearly along the suction and pressure sides of the blades. There are no changes made to the meshing settings used in the mesh of the test case CFD. Looking at the ξ contours taken from Plane 6, given in Fig.11, shows discouraging results with increased vortex size and strength and an increased lift off distance of the passage vortex with a 21.09mm lift off.

Upon examining the development of vortices in the passage, it is seen that the large radius in the

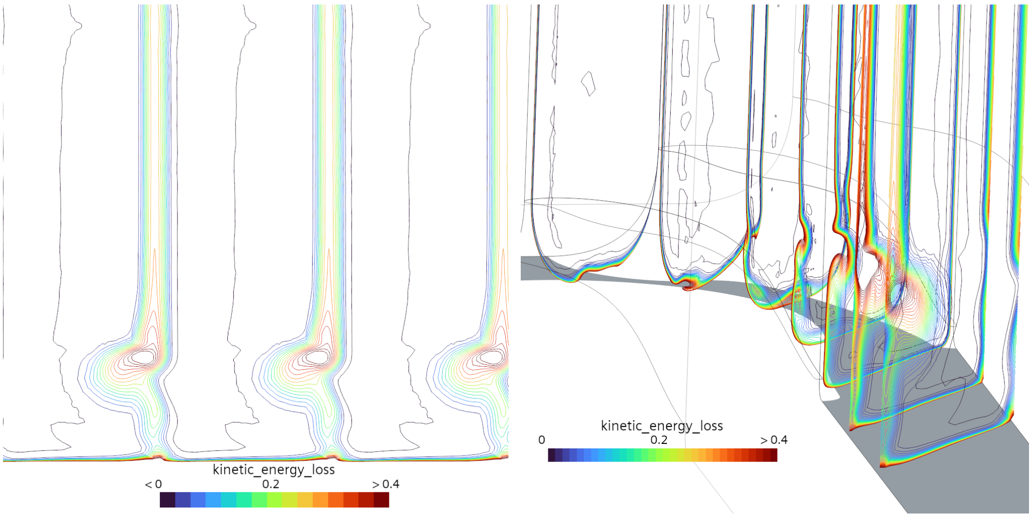

Figure 11: Kinetic Energy Loss Coefficient (ξ) Contour With the Fillet Feature (Left) Kinetic Energy Loss Coefficient (ξ) Contours Along the Passage (Right)

leading edge creates bigger vortices by causing more of the boundary layer to start turning either side of the blade. In the end this creates a larger passage vortex with overall more losses. The Feature seems to also combine other vortical structures together by funneling them thorough the narrow passage, which could also be a contributor to the results seen in Fig.11.

CFD Studies Of The Channel Feature

For this study a channel feature is added to the passage. This channel goes down in to the endwall at the passage inlet and merges back with the passage at the exit. Channel is implemented in such a way that the walls of the channel stays in between the suction and pressure side blades. A view of this feature can be seen in Fig.12. The endwall is shown transparently for clarity. Channel has an inlet width of 16.5mm and an outlet width of 13.5mm. It is not connected to the passage tangentially which means there is a discontinuity at the surface at the inlet and outlet edges. There is no changes made to the meshing settings used in the mesh of the test case CFD provided in methodology section, except the total thickness of the boundary layer mesh and the number of boundary layers are reduced at the channel walls, to prevent intersecting layers from collapsing and keep a uniform wall thickness for the entire mesh. Close up of the mesh inside the channel can be seen in Fig.12.

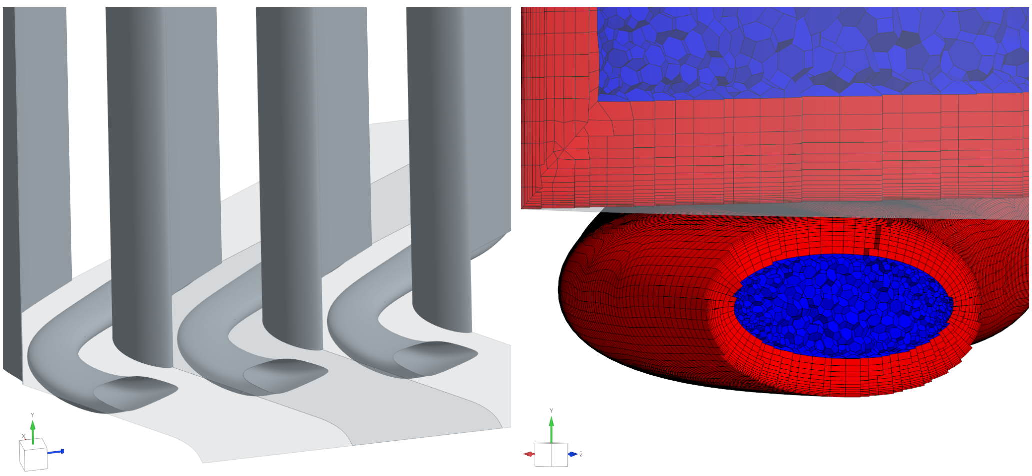

Figure 12: Channel Feature (Left) Generated Mesh (Right)

Upon examining the results obtained with the channel it is seen that the passage vortex is significantly smaller but the lift off distance of the vortex is increased to about 18mm. The reason for this can be attributed to the fact that the channel scoops some of incoming flow including the boundary layer, which prevents passage vortex from strengthening. The lift off issue could be attributed to the construction of the channel geometry. As mentioned before, there is a discontinuity between the endwall surface and the channel wall which causes more vortices to emerge. This can cause increased lift off distance and reduce the effectiveness of the loss reduction. These effects can be seen in Fig.13.

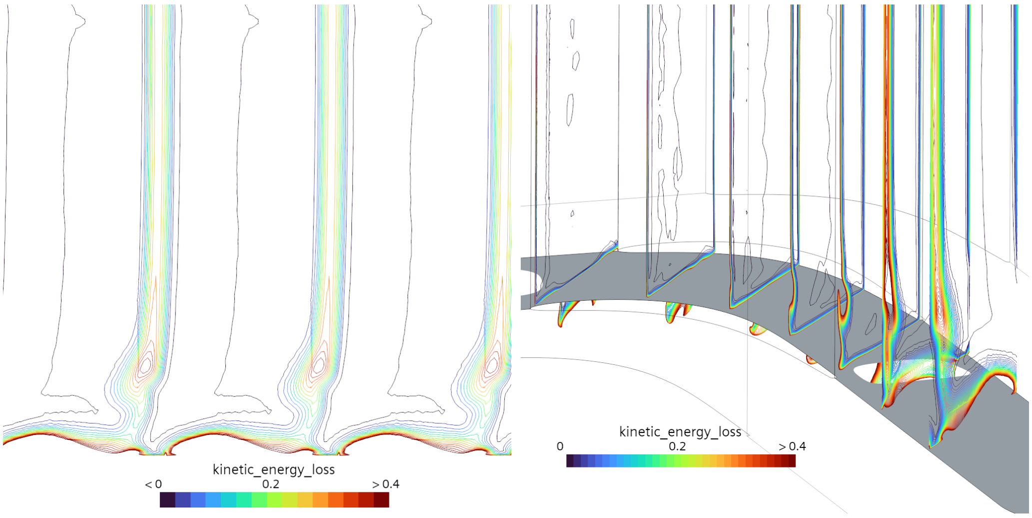

Figure 13: Kinetic Energy Loss Coefficient (ξ) Contour With the Channel Feature (Left) Kinetic Energy Loss Coefficient (ξ) Contours Along the Passage (Right)

From examining the kinetic energy loss at the passage, we can see the effect the channel exit has on the flow. This could be caused by the existing vortical flow structures inside the channel, which is caused by the discontinuity at the inlet of the channel.

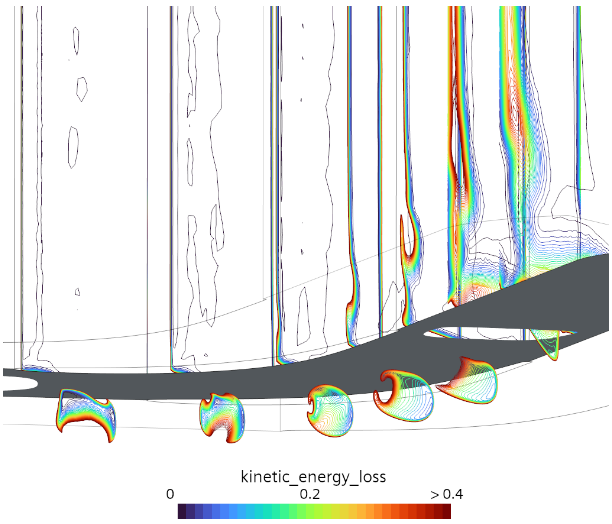

Figure 14: Kinetic Energy Loss Coefficient (ξ) Contours Plotted Inside the Channel

The ξ contours at the channel can be seen in Fig.14. It is evident that there is a big vortex structure in the channel. This vortex merging with the passage causes extra losses to emerge at Plane 6. This channel vortex could be the main contributor to the increased lift off distance and possibly hinders the loss reduction capabilities. These effects of the channel feature needs further investigation.

Kinetic Energy Loss Coefficient Comparison

Behavior of the passage vortex with different endwall features are examined in the previous sections. To quantitatively compare the different features, their mass flow averaged ξ profiles with respect to the non dimensional spanwise direction are given in Fig.15. Mass flow averaging is done by taking mass flow average of the total pressure terms and taking the area average of the static pressure terms in the pitchwise direction. These terms can be found in Eqn.1.

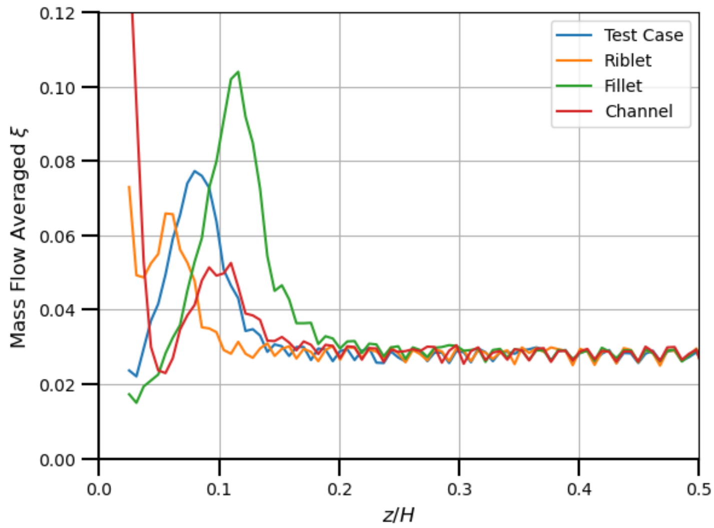

Figure 15: Mass Flow Averaged Kinetic Energy Loss Coefficient (ξ) With Respect to Spanwise Location

From the graph it can be observed that the examined features, in their current design, show significant alterations in the loss profiles. Channel and riblet features are able to reduce the size of the passage vortex to increase efficiency. Channel and riblet features provide roughly 32% and 25% reduction in kinetic energy loss, respectively. Fillet feature on the other hand is causing the passage vortex to grow and move away from the endwall. It is observed that, fillet feature with its current design causes an increase of about 25% in kinetic energy loss. It can also be observed that there are additional losses introduced by the riblet and channel feature closer to the endwall. These losses occur due to vortex structures examined in the previous sections.

CONCLUSIONS

In this work, a new design space enabled by advanced manufacturing techniques such as additive layer manufacturing has been numerically explored to reduce of secondary flow losses present in turbomachinery.

A novel endwall modification, incorporating a channel through the cascade passage, has been investigated. Experimental data from a low-pressure turbine linear cascade have been used as a validation case for the numerical methodology and served as the baseline, alongside conventional endwall contouring methods, namely riblets and fillets. The results show that the channel feature reduces the kinetic energy loss coefficient in the secondary flow core by approximately 32%, outperforming the conventional endwall contouring approaches.

Overall, this new design space enabled by advanced manufacturing techniques offers promising potential for reducing secondary flows and improving efficiency. As future work, this novel endwall feature could serve as a baseline case for optimization studies to further improve its effectiveness. High-fidelity simulations may also be employed to capture more detailed flow physics.

References

Denton, J. D. (2009) *The 1993 IGTI Scholar Lecture: Loss Mechanisms in Turbomachines*, Journal of Turbomachinery, Vol. 115, p: 621-656, Oct 1993

Dickel, Jacob A. and Marks, Christopher and Clark, John and Sondergaard, Rolf and Wolff, Mitch (2018) *Non-Axisymmetric Endwall Contouring of Front-Loaded High-Lift Low Pressure Turbines*, AIAA Aerospace Sciences Meeting, Jan 2018

Langston, L.S. (2001) *Secondary Flows in Axial Turbines—A Review*, Annals of the New York Academy of Sciences, Vol. 434, p: 11-26, May 2001

Langtry, R. B. and Menter, F. R. (2009) *Correlation-Based Transition Modeling for Unstructured Parallelized Computational Fluid Dynamics Codes*, AIAA Journal, Vol. 47, p: 2894-2906, May 2012

Lavagnoli, Sergio and Lopes, Gustavo and Simonassi, Loris and Torre, Antonino Federico Maria (2024) *SPLEEN - High Speed Turbine Cascade – Test Case Database*, Zenodo, Dec 2023

Lopes D. C. and Filipe G. (2024) *Aerodynamics of a High-Speed Low-Pressure Turbine Cascade with Unsteady Wakes and Purge Flow*, Phd Thesis, Université de Liège [BE] [Faculté des Sciences Appliquées], Aug 2024

Marconcini, M. and Pacciani, R. and Arnone, A. and Michelassi, V. and Pichler, R. and Zhao, Y. and Sandberg, R. (2019) *Large Eddy Simulation and RANS Analysis of the End-Wall Flow in a Linear Low-Pressure-Turbine Cascade—Part II: Loss Generation*, Journal of Turbomachinery, Vol. 141, Jan 2019

Pichler, R. and Zhao, Y. and Sandberg, R. and Michelassi, V. and Pacciani, R. and Marconcini, M. and Arnone, A. (2019) *Large-Eddy Simulation and RANS Analysis of the End-Wall Flow in a Linear Low-Pressure Turbine Cascade, Part I: Flow and Secondary Vorticity Fields Under Varying Inlet Condition*, Journal of Turbomachinery, Vol. 141, Nov 2019

Rosafio, N. and Lopes, G. and Salvadori, S. and Lavagnoli, S. and Misul, D. A. (2014) *RANS Prediction of Losses and Transition Onset in a High-Speed Low-Pressure Turbine Cascade*, Energies, Vol. 16, Oct 2023

Saha, Arun K. and Mahmood, Gazi I. and Acharya, Sumanta (2006) *The Role of Leading-Edge Contouring on End-Wall Flow and Heat Transfer: Computations and Experiments*, Turbo Expo, Vol. 3, p: 1105-1118, Sep 2008

Sauer , H. and Müller , R. and Vogeler, K. (2000) *Reduction of Secondary Flow Losses in Turbine Cascades by Leading Edge Modifications at the Endwall*, Journal of Turbomachinery, Vol. 123, p: 207-213, Feb 2000

Miao, X. and Zhang, Q. and Jiang, H. and Qi, H. (2014) *Application of Riblets on Turbine Blade Endwall Secondary Flow Control*, Turbo Expo, Vol. 2C, Sep 2014